Supplementary Figure 1

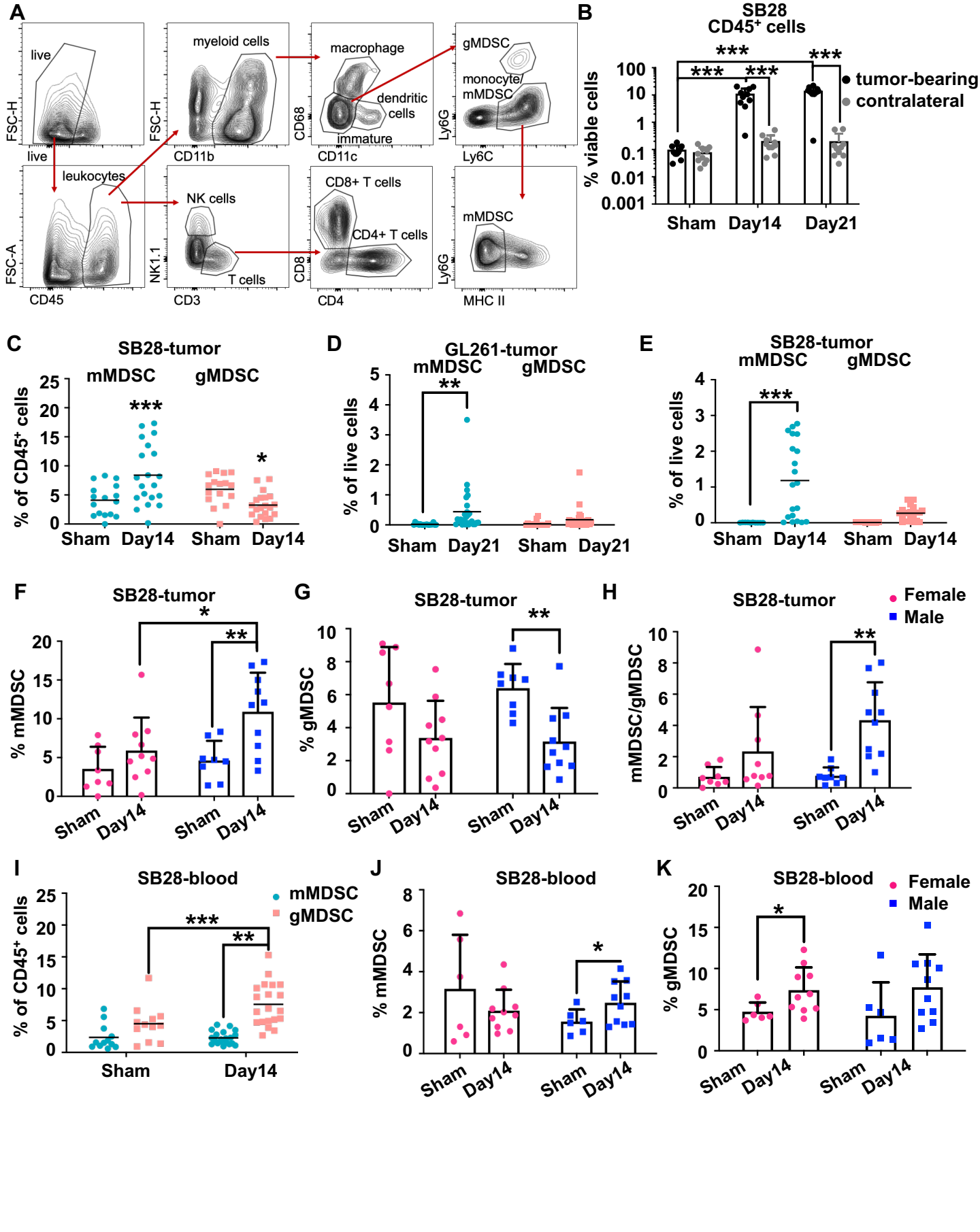

Supplementary Figure 1. Increased mMDSC frequency in tumors associates with poor prognosis. **A,** Contour plots demonstrating the gating strategy of immune populations from tumors. **B,** Frequency of $CD45^{high}$ bone marrow-derived immune cells in resected tumors versus the contralateral hemisphere of sham-injected or 20,000 SB28-implanted mice on day 14 and day 21. Data shown as mean ± s.d. of n = 9-10/group. *** p<0.001 as determined by two-way ANOVA. **C,** Percentage of mMDSCs ($CD11b^+CD68^-Ly6C^+Ly6G^-I\text{-}A/I\text{-}E^-$, $CD11b^+CD68^-Ly6C^+Ly6G^-$ or $CD11b^+F4/80^-Ly6C^+Ly6G^-$) and gMDSCs ($CD11b^+CD68^-Ly6C^-Ly6G^+$ or $CD11b^+F4/80^-Ly6C^-Ly6G^+$) in $CD45^+$ cells of the left hemisphere from n = 16 sham-injected and n = 20 SB28-bearing animals. Data shown for individual mice combined from two independent experiments, and * p<0.05, *** p<0.001 as calculated by unpaired t-test. **D,** Percentage of mMDSCs and gMDSCs as a fraction of live cells of the left hemisphere from n = 18 sham-injected and n = 26 GL261-bearing animals. Data shown for individual mice combined from three independent experiments, and ** p<0.01 as determined by two-way ANOVA. **E,** Percentage of mMDSCs and gMDSCs as a fraction of the live cells of the left hemisphere from n = 10 sham-injected and n = 20 SB28-bearing animals. Data shown for individual mice combined from two independent experiments, and *** p<0.001 as determined by two-way ANOVA. **F,** Percentage of mMDSCs in the left hemisphere 14 days post-SB28 implantation or sham injection. Data shown as mean ± s.d. from n = 8 sham-injected and n = 10 SB28-bearing mice per sex combined from two independent experiments and * p<0.05, ** p<0.01 as determined by unpaired t-test. **G,** Percentage of gMDSCs in the left hemisphere 14 days post-SB28 implantation or sham injection. Data shown as mean ± s.d. from n = 8 sham-injected and n = 10 SB28-bearing mice per sex combined from two independent experiments. ** p<0.01 as determined by unpaired t-test. **H,** Ratio of mMDSCs to gMDSCs in the left hemisphere 14 days post-SB28 implantation or sham injection. Data combined from two independent experiments was shown as mean ± s.d. from n = 8 sham-injected and n = 9-10 SB28-bearing mice per sex. ** p<0.05, ** p<0.01 as determined with unpaired t-test. **I,** Percentage of mMDSCs and gMDSCs in the systemic circulation of n = 12 sham-injected and n = 20 SB28-bearing animals. Data shown from two independent experiments for individual animals and ** p<0.01, *** p<0.001 as calculated by unpaired t-test. **J,** Percentage of mMDSCs in the circulation of sham-injected and SB28-bearing mice on day 14. Data shown as mean ± s.d. from two independent experiments. n = 6 sham-injected and n = 10 SB28-bearing mice per sex and * p<0.05 as determined by unpaired t-test. **K,** Percentage of gMDSCs in the circulation of sham-injected and SB28-bearing mice on day 21. Data shown as mean ± s.d. from three independent experiments. n = 6 sham-injected and n = 10 GL261-bearing mice per sex and * p<0.05 as determined by unpaired t-test.

Supplementary Figure 2

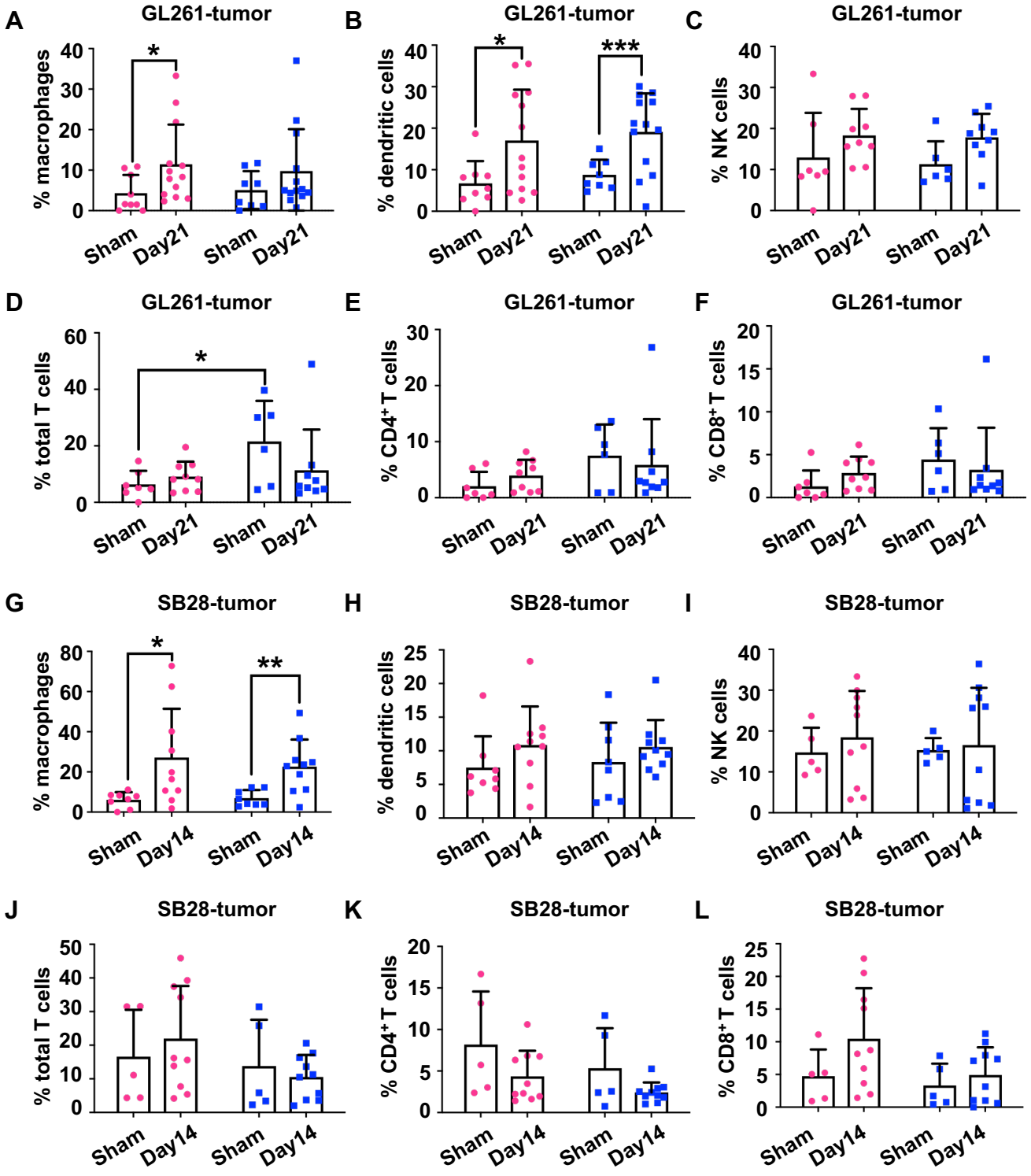

Supplementary Figure 2. The frequency of nonMDSC tumor-infiltrating immune populations is similar between males and females. **A-F,** Frequency of tumor-infiltrating immune populations 21 days post-GL261 implantation or sham injection shown as mean ± s.d. **(A)** Percentage of macrophages ($CD11b^+CD68^+$ or $CD11b^+F4/80^+$) from n = 8-9 sham control mice and n = 13 tumor-bearing mice. Data shown from three independent experiments, and * $p<0.05$ as determined by unpaired t-test. **(B)** Percentage of myeloid dendritic cells ($CD11b^+CD11c^+$) from n = 8-9 sham control mice and n = 13 tumor-bearing mice. Data shown from three independent experiments and *** $p<0.001$, * $p<0.05$ as determined by unpaired t-test. **(C)** Percentage of natural killer cells ($CD3^-NK1.1^+$) from n = 6-7 sham control mice and n = 9 tumor-bearing mice. Data shown from two independent experiments. **(D)** Percentage of total T cells ($CD3^+NK1.1^-$) from n = 6 sham control mice and n = 9 tumor-bearing mice. Data shown from two independent experiments. **(E)** Percentage of $CD4^+$ T cells ($CD3^+CD4^+CD8^-$) from n = 6-7 sham control mice and n = 9 tumor-bearing mice. Data shown from two independent experiments. **(F)** Percentage of $CD8^+$ T cells ($CD3^+CD8^+CD4^-$) from n = 6-7 sham control mice and n = 9 tumor-bearing mice. Data shown from two independent experiments. **G-L,** Frequency of tumor-infiltrating immune populations 14 days post-SB28 implantation or sham injection shown as mean ± s.d. **(G)** Percentage of macrophages ($CD11b^+CD68^+$) from n = 7 sham-injected and n = 10 SB28-bearing mice per sex. Data shown from two independent experiments, and * $p<0.05$, ** $p<0.01$ as determined by unpaired t-test. **(H)** Percentage of myeloid dendritic cells ($CD11b^+CD11c^+$) from n = 7 sham-injected and n = 10 SB28-bearing mice per sex. Data shown from two independent experiments. **(I)** Percentage of natural killer cells ($CD3^-NK1.1^+$) from n = 5 sham-injected and n = 10 SB28-bearing mice per sex. Data shown from two independent experiments. **(J)** Percentage of total T cells ($CD3^+NK1.1^-$) from n = 5 sham-injected and n = 10 SB28-bearing mice per sex. Data shown from two independent experiments. **(K)** Percentage of $CD4^+$ T cells ($CD3^+CD4^+CD8^-$) from n = 5 sham-injected and n = 10 SB28-bearing mice per sex. Data shown from two independent experiments. **(L)** Percentage of $CD8^+$ T cells ($CD3^+CD8^+CD4^-$) from n = 5 sham-injected and n = 10 SB28-bearing mice per sex. Data shown from two independent experiments.

Supplementary Figure 3

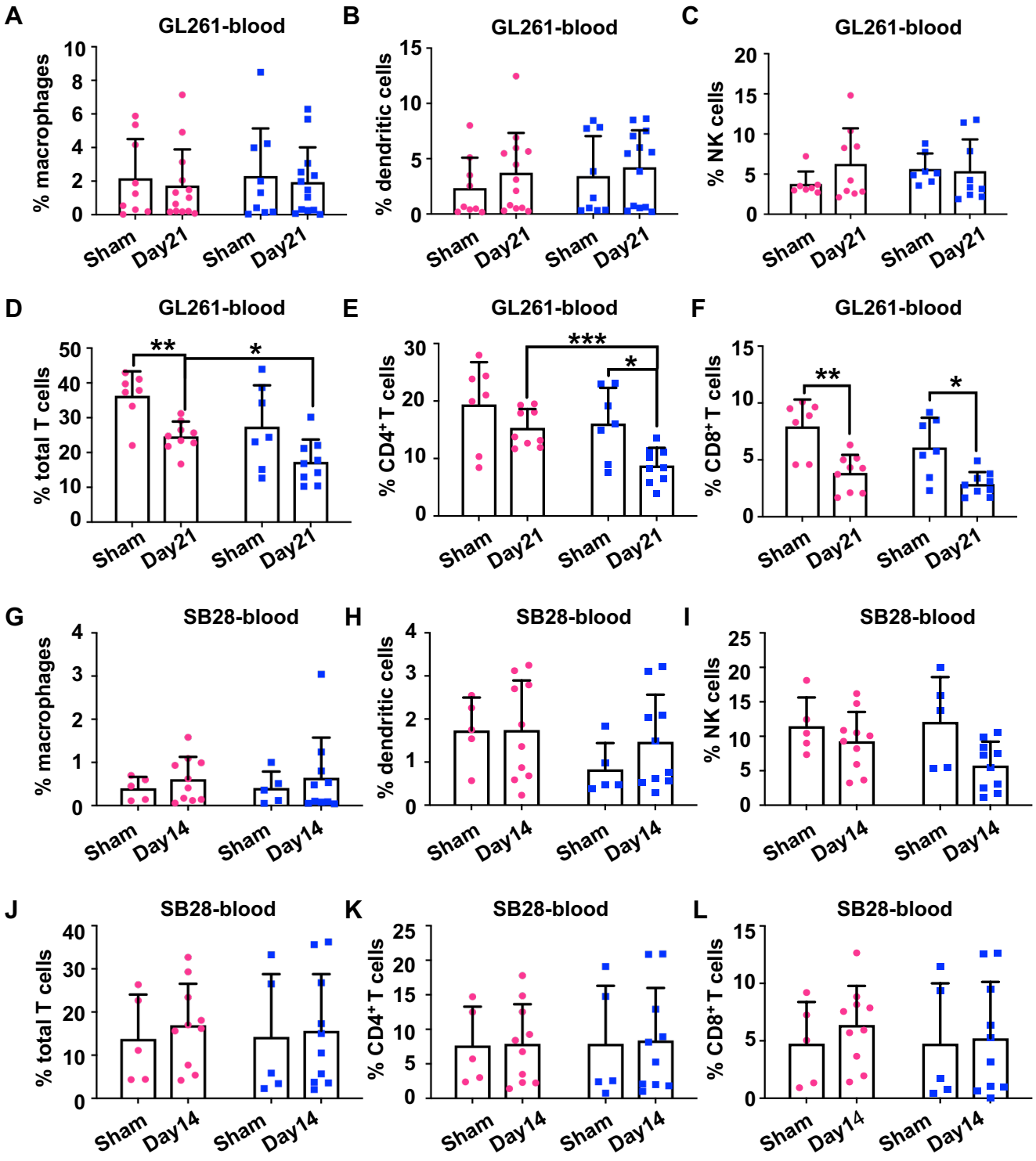

Supplementary Figure 3. Increase in the systemic levels of immune cells is limited to gMDSCs. **A-F,** Frequency of circulating immune populations 21 days post-GL261 implantation or sham injection shown as mean ± s.d. **(A)** Percentage of macrophages ($CD11b^+CD68^+$ or $CD11b^+F4/80^+$) from n = 9 sham control mice and n = 13 tumor-bearing mice. Data shown from three independent experiments. **(B)** Percentage of myeloid dendritic cells ($CD11b^+CD11c^+$) from n = 9 sham control mice and n = 13 tumor-bearing mice. Data shown from three independent experiments. **(C)** Percentage of natural killer cells ($CD3^-NK1.1^+$) from n = 7 sham control mice and n = 9 tumor-bearing mice. Data shown from two independent experiments. **(D)** Percentage of total T cells ($CD3^+NK1.1^-$) from n = 6-7 sham control mice and n = 9 tumor-bearing mice. Data shown from two independent experiments, and * $p<0.05$, ** $p<0.01$ as determined by unpaired t-test. **(E)** Percentage of $CD4^+$ T cells ($CD3^+CD4^+CD8^-$) from n = 7 sham control mice and n = 9 tumor-bearing mice. Data shown from two independent experiments, and * $p<0.05$, *** $p<0.001$ as determined by unpaired t-test. **(F)** Percentage of $CD8^+$ T cells ($CD3^+CD8^+CD4^-$) from n = 7 sham control mice and n = 9 tumor-bearing mice. Data shown from two independent experiments, and * $p<0.05$, ** $p<0.01$ as determined by unpaired t-test. **G-L,** Frequency of circulating immune populations 14 days post-SB28 implantation or sham injection shown as mean ± s.d. **(G)** Percentage of macrophages ($CD11b^+CD68^+$) from n = 5 sham-injected and n = 10 SB28-bearing mice per sex. Data shown from two independent experiments. **(H)** Percentage of myeloid dendritic cells ($CD11b^+CD11c^+$) from n = 5 sham-injected and n = 10 SB28-bearing mice per sex. Data shown from two independent experiments. **(I)** Percentage of natural killer cells ($CD3^-NK1.1^+$) from n = 5 sham-injected and n = 10 SB28-bearing mice per sex. Data shown from two independent experiments. **(J)** Percentage of total T cells ($CD3^+NK1.1^-$) from n = 5 sham-injected and n = 10 SB28-bearing mice per sex. Data shown from two independent experiments. **(K)** Percentage of $CD4^+$ T cells ($CD3^+CD4^+CD8^-$) from n = 5 sham-injected and n = 10 SB28-bearing mice per sex. Data shown from two independent experiments. **(L)** Percentage of $CD8^+$ T cells ($CD3^+CD8^+CD4^-$) from n = 5 sham-injected and n = 10 SB28-bearing mice per sex. Data shown from two experiments.

Supplementary Figure 4

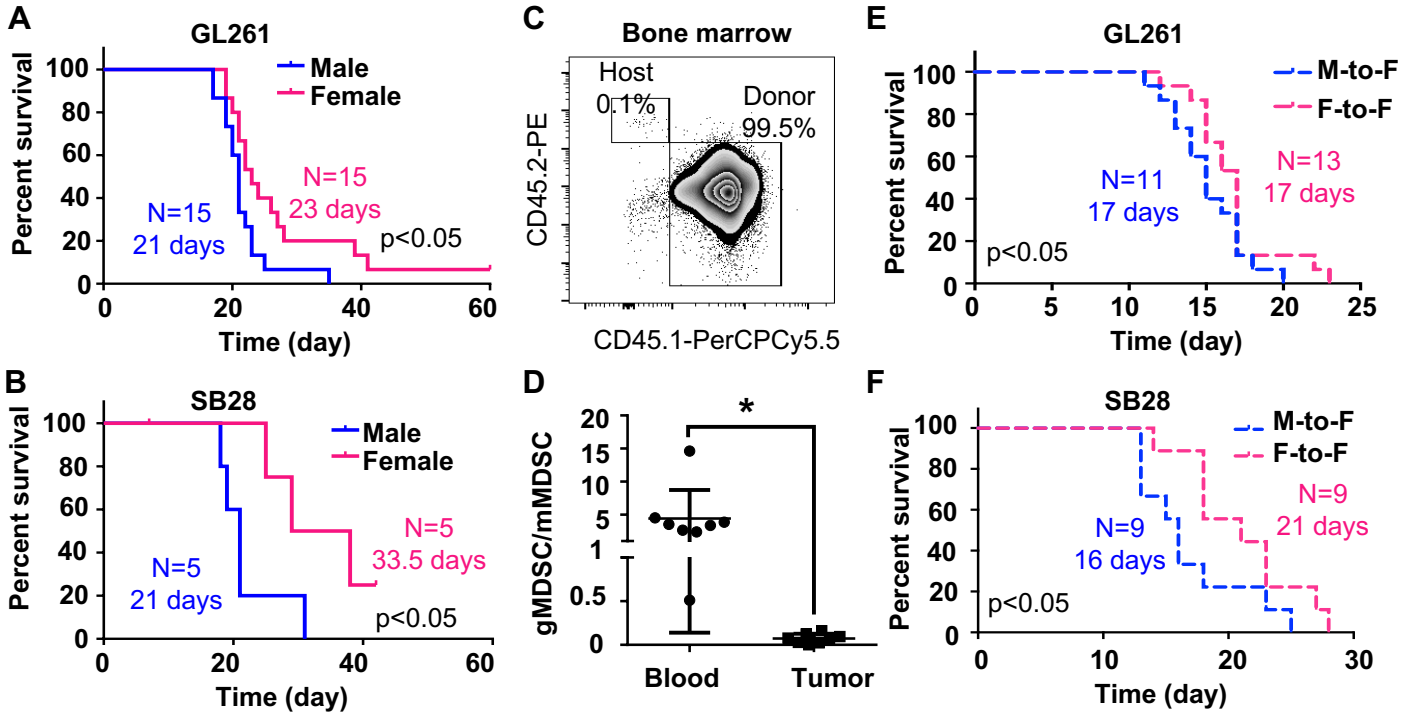

Supplementary Figure 4. Male-to-female bone marrow transplantation transfers the survival disadvantage observed in males. **A,** Kaplan-Meier curves depicting relative survival of male versus female mice orthotopically implanted with 25,000 GL261 cells. Data combined from three independent experiments with n = 15 females and n = 15 males. $p<0.05$ as determined by Gehan–Breslow–Wilcoxon test. **B,** Kaplan-Meier curves depicting relative survival of male versus female mice orthotopically implanted with 20,000 SB28 cells. Data representative of independent experiments with n = 5 females and n = 5 males. $p<0.05$ as determined by Gehan–Breslow–Wilcoxon test. **C,** Representative zebra plot demonstrating the efficacy of bone marrow transplantation at experimental endpoint. **D,** Ratio of mMDSCs to gMDSCs at experimental endpoint in blood and tumor of bone marrow-transplanted mice implanted with GL261. Data combined from n = 4 female-to-female and n = 4 male-to-female mice. $p<0.05$ as determined by unpaired t-test. **E,** Kaplan-Meier curves depicting survival of female mice transplanted with bone marrow from male or female donors. Four weeks after the transplantation procedure, mice were intracranially injected with 10,000 GL261 cells. Data shown from n = 11 male-to-female and n = 13 female-to-female bone marrow-transplanted mice. $p<0.05$ as determined by Gehan–Breslow–Wilcoxon test. **F,** Kaplan-Meier curves depicting survival of female mice transplanted with bone marrow from male or female donors. Four weeks after the transplantation procedure, mice were intracranially injected with 5,000 SB28 cells. Data shown from n = 9 male-to-female and female-to-female bone marrow-transplanted mice. $p<0.05$ as determined by Gehan–Breslow–Wilcoxon test.

Supplementary Figure 5

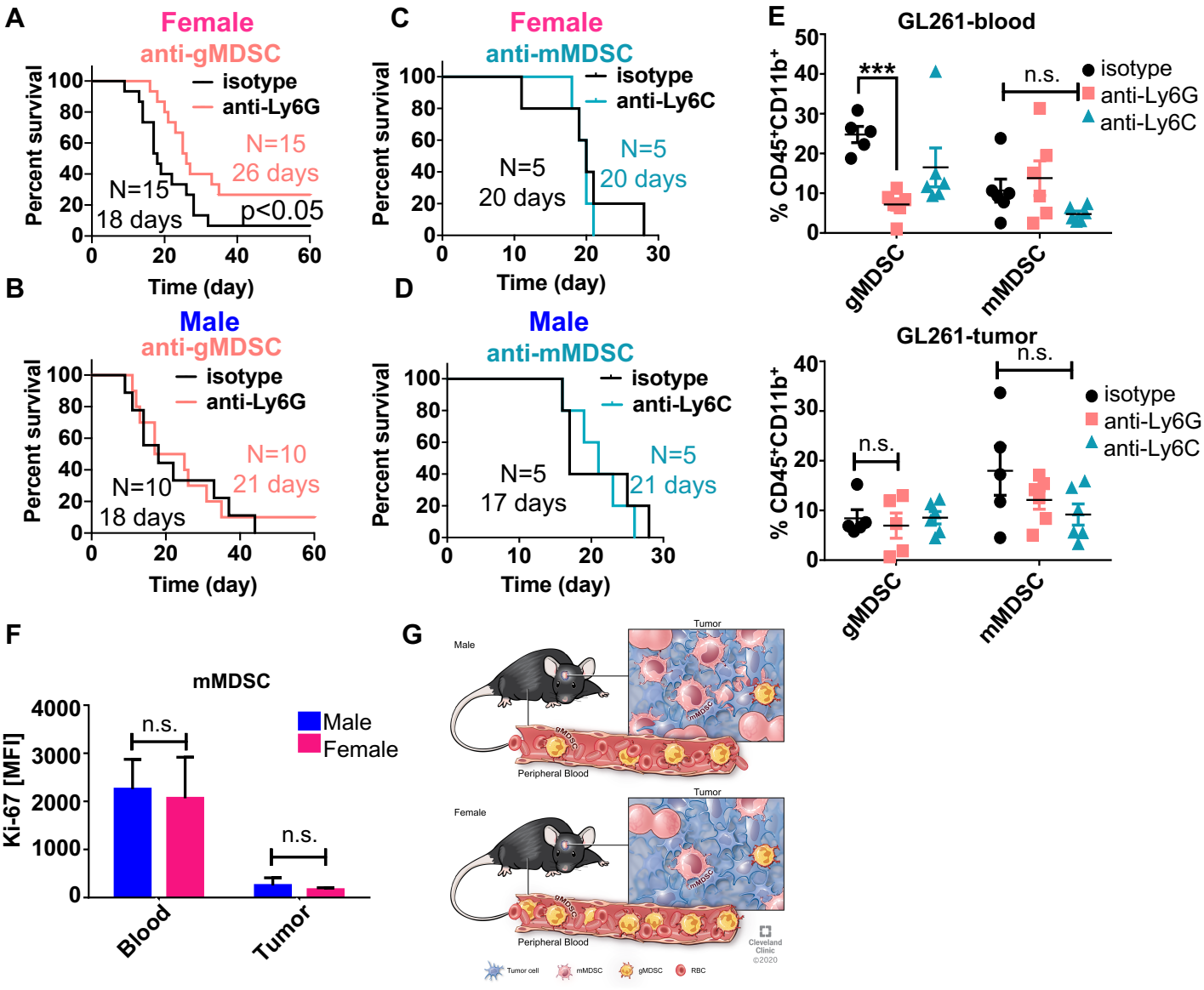

Supplementary Figure 5. gMDSC depletion is effective in females, while lack of efficacy in mMDSC depletion could be driven by active cell proliferation. **A-D,** Kaplan-Meier curves depicting survival of female and male mice treated with (**A-B**) anti-Ly6G and (**C-D**) anti-Ly6C neutralizing antibodies every other day starting 7 days post-SB28 implantation compared to isotype-treated mice. For **A,** n = 15 for isotype- and n = 15 for anti-Ly6G-treated female mice; for **B,** n = 10 for isotype- and n = 10 for anti-Ly6G-treated male mice; for **C,** n = 5 for isotype- and n = 5 for anti-Ly6C-treated female mice; for **D,** n = 5 for isotype- and n = 5 for anti-Ly6C-treated male mice. Data combined from one to three independent experiments. Significance was determined by Gehan–Breslow–Wilcoxon test, with $p<0.05$ considered a significant difference. **E,** Percentage of mMDSCs and gMDSCs from blood (left) and tumor (right) of tumor-bearing mice at experimental endpoint. Data shown as mean ± s.d. of n = 5-6 (2-3 male/3 female) for isotype-, n = 5-6 (3 male/2-3 female) for anti-Ly6G- and n = 6 (4 male/2 female) for anti-Ly6C-treated mice. *** $p<0.001$ as determined by unpaired Student's t-test. **F,** Comparison of Ki-67 intensity of mMDSCs isolated from n = 3 mice. Data shown as mean ± s.d. and statistical analysis performed with paired t-test. **G,** Proposed mechanism of differential mMDSC versus gMDSC accumulation in male and female mice.

Supplementary Figure 6

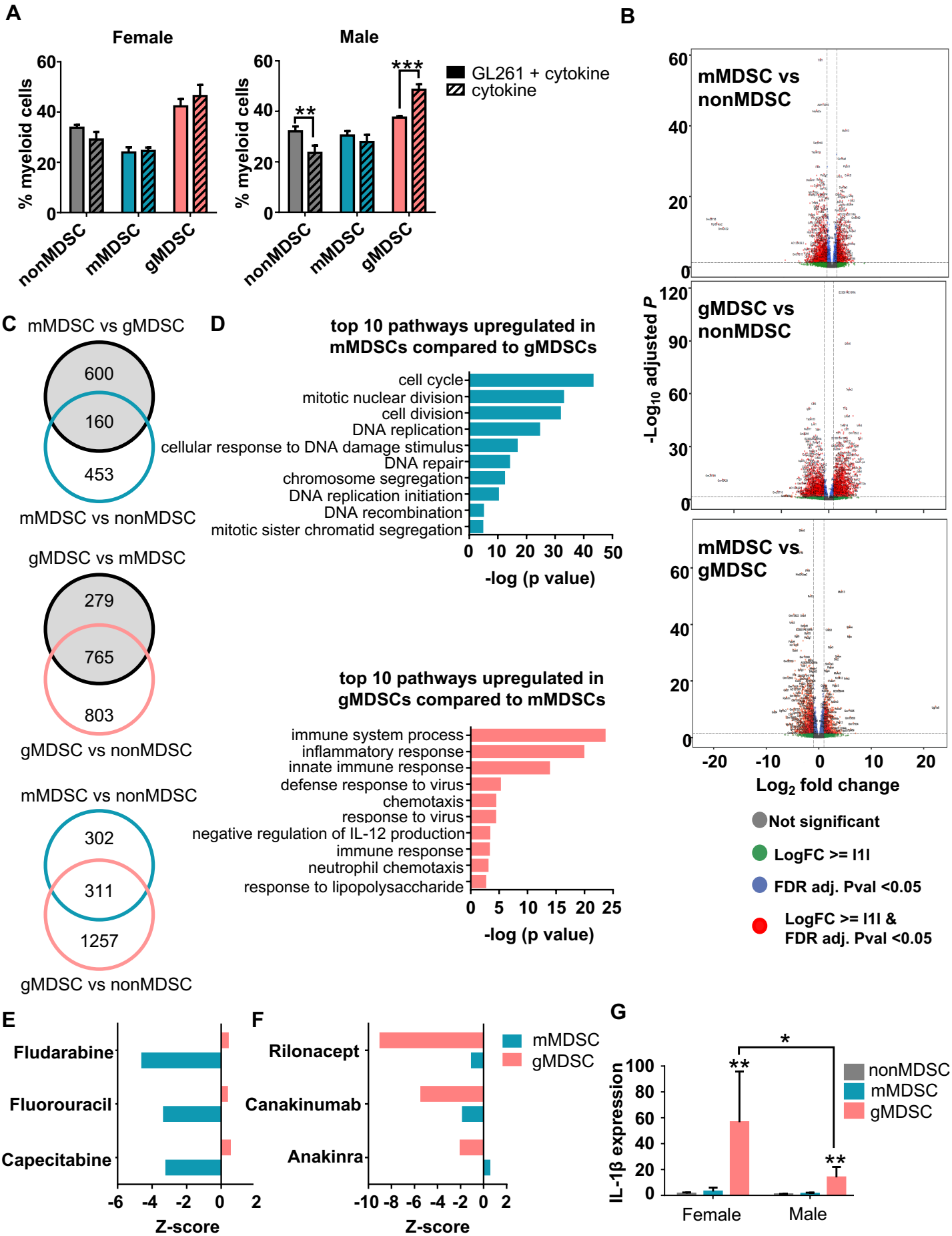

Supplementary Figure 6. In vitro-generated mMDSCs and gMDSCs have different gene expression profiles. **A,** Comparison of the polarization efficacy of mMDSCs and gMDSCs generated via co-culture approach or by cytokine stimulation. Data shown as mean ± s.d. from n = 3 females (left) and males (right). **B,** Volcano plots demonstrating the differential gene expression signature of mMDSC, gMDSC and nonMDSC fractions from n = 6 biological replicates. **C,** Number of differentially upregulated genes in mMDSCs (top) and gMDSCs (middle) in comparison to the other MDSC subset and control. Genes upregulated in both MDSC subsets (bottom) from n = 6 biological replicates. **D,** Top 10 differentially regulated pathways between mMDSCs and gMDSCs using GeneOntology Enrichment Analysis. **E,** Comparison of the specificity of fludarabine to the chemotherapeutic agents used to target immunosuppression in GBM (Otvos et al., *Stem Cells*, 2016 & Alban et al., *JCI Insight*, 2019). **F,** Specificity of the multiple IL-1 pathway inhibitors predicted to target gMDSCs by network medicine analysis. **G,** Fold difference in IL-1β expression in MDSC subsets compared to nonMDSCs. Data shown as mean ± s.d. from n = 3 male versus female mice. $p<0.05$, ** $p<0.01$ as determined by unpaired t-test.

Supplementary Figure 7

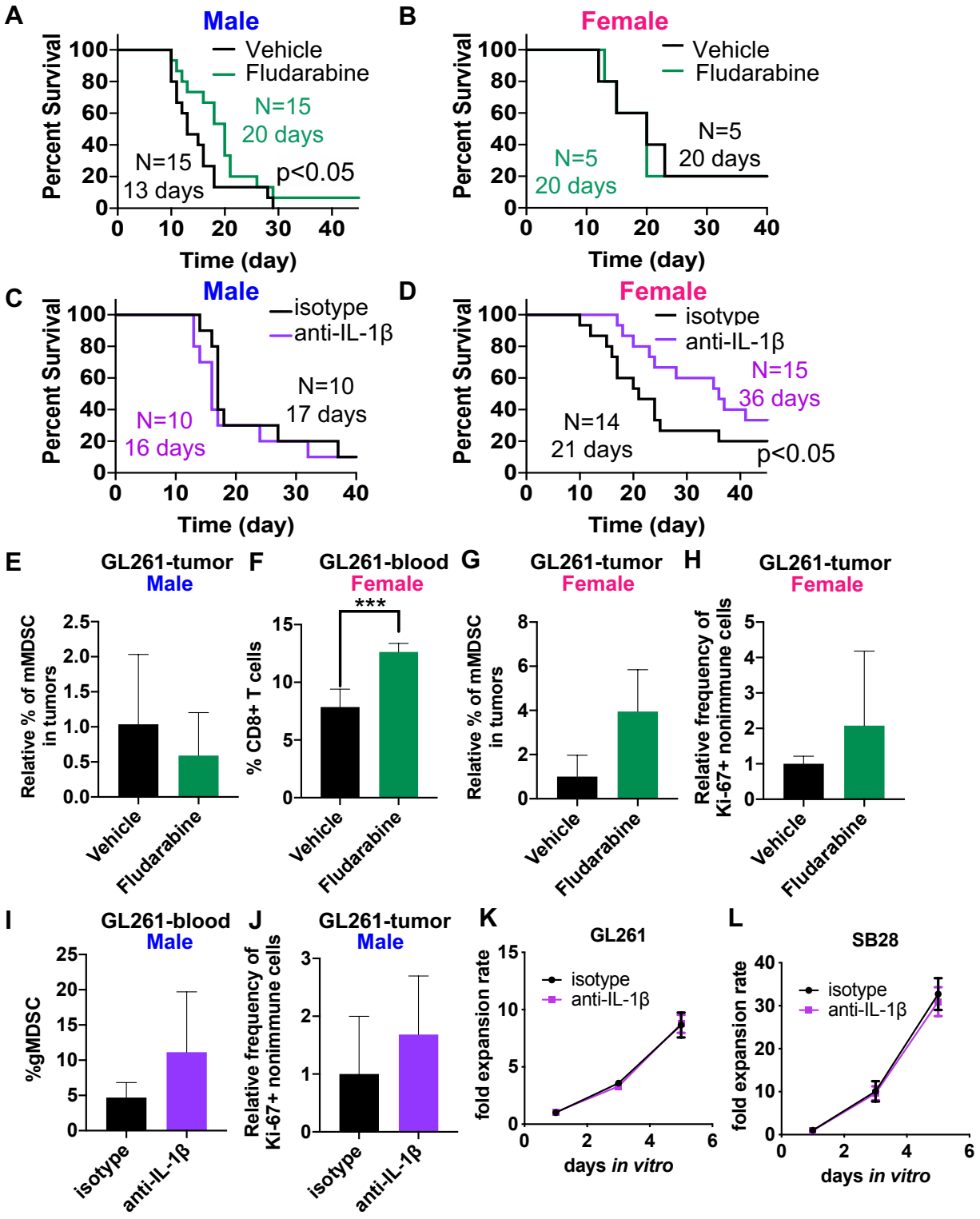

Supplementary Figure 7. mMDSC targeting by fludarabine benefits males, while gMDSC interference with anti-IL-1β antibody improves the survival of female mice. Kaplan-Meier curves depicting survival of **A,** male and **B,** female SB28-bearing mice treated with fludarabine. Data presented from one-three independent experiments with (**A**) n = 15 vehicle-treated males and n = 15 fludarabine-treated males, (**B**) n = 5 vehicle-treated females and n = 5 fludarabine-treated females. $p<0.05$ as determined by Gehan–Breslow–Wilcoxon test. Kaplan-Meier curves depicting survival of **C,** male and **D,** female SB28-bearing mice treated with anti-IL1β neutralizing or isotype control antibody. Data presented from two-three independent experiments with (**C**) n = 10 isotype control-treated males and n = 10 anti-IL-1β antibody-treated males and (**D**) n = 15 isotype control-treated females and n = 15 anti-IL-1β antibody-treated females. $p<0.05$ as determined by Gehan–Breslow–Wilcoxon test. **E,** Percentage of tumor-infiltrating mMDSCs as a fraction of live cells in n = 8 vehicle and n = 6 fludarabine-treated GL261-bearing male mice after two cycles. Data shown from two independent experiments and normalized to vehicle control . **F,** Frequency of CD8+ T cells in the circulation of n = 5 vehicle- and n = 4 fludarabine-treated GL261-bearing female mice. Data shown as mean ± s.d., and *** $p<0.001$ as calculated by unpaired t-test. **G,** Percentage of tumor-infiltrating mMDSCs as a fraction of live cells in n = 5 vehicle and n = 5 fludarabine-treated GL261-bearing female mice after two cycles. Data shown as mean ± s.d. and normalized to vehicle control. **H,** Percentage of Ki-67+ cells in the nonimmune cells of the left hemisphere from n = 5 vehicle and n = 5 fludarabine-treated GL261-bearing female mice after two cycles. Data shown as mean ± s.d. and normalized to vehicle control. **I,** Frequency of gMDSCs in the circulation of n = 5 isotype- and n = 5 anti-IL-1β-treated GL261-bearing male mice. Data shown as mean ± s.d. **J,** Percentage of Ki-67+ cells in the nonimmune cells of the left hemisphere from n = 5 isotype- and n = 5 anti-IL-1β-treated GL261-bearing male mice after two cycles. Data shown as mean ± s.d. normalized to isotype control. Proliferation rate of **K,** GL261 and **L,** SB28 cells treated with anti-IL-1β or isotype control on days 1, 3 and 5 in triplicate. The values shown are relative to isotype control on day 1.

Supplementary Figure 8

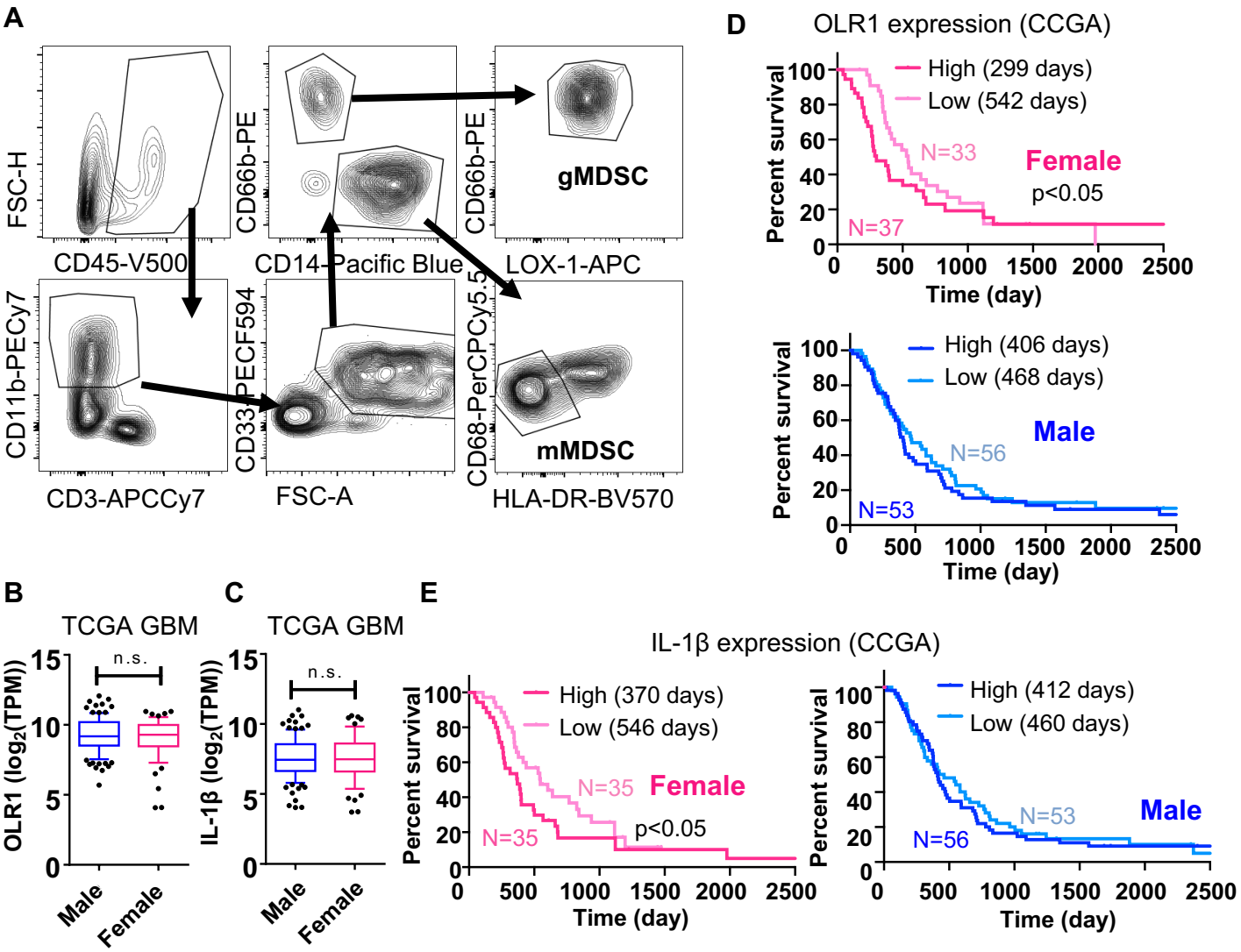

Supplementary Figure 8. MDSC gating strategy for flow cytometry and bioinformatic analysis of gMDSC signatures. **A,** Gating strategy for the analysis of tumor-infiltrating mMDSCs and gMDSCs from patients with GBM. LOX-1 positivity of gMDSCs was determined based on expression levels in mMDSCs. **B,** OLR1 TPM expression values from the TCGA GBM dataset. Data shown as box and whiskers from n = 107 male and n = 59 female patients. Comparison is based on unpaired Student's t-test. **C,** IL-1β TPM expression values from the TCGA GBM dataset. Data shown as box and whiskers from n = 107 male and n = 59 female patients. Comparison is based on unpaired Student's t-test. **D,** Correlation among OLR1 expression levels, patient sex and survival duration was analyzed via the Chinese Glioma Gene Atlas (CGGA) database in IDH-wild type primary GBM patients. High and low expression levels were determined based on median expression. Data shown for n = 37 female patients with high OLR1 expression and n = 33 female patients with low OLR1 expression (top) and for n = 53 male patients with high OLR1 expression and n = 56 male patients with low OLR1 expression (bottom). $p<0.01$ as determined by Gehan–Breslow–Wilcoxon test. **E,** Correlation among IL-1β expression levels, patient sex and survival duration was analyzed via CCGA database in patients with IDH-wild type primary GBM. High and low expression levels were determined based on median expression. Data shown for n = 35 female patients with high IL-1β expression and n = 35 female patients with low IL-1β expression (left) and for n = 56 male patients with high IL-1β expression and n = 53 male patients with low IL-1β expression (right). $p<0.05$ as determined by Gehan–Breslow–Wilcoxon test.

Supplementary Figure 9

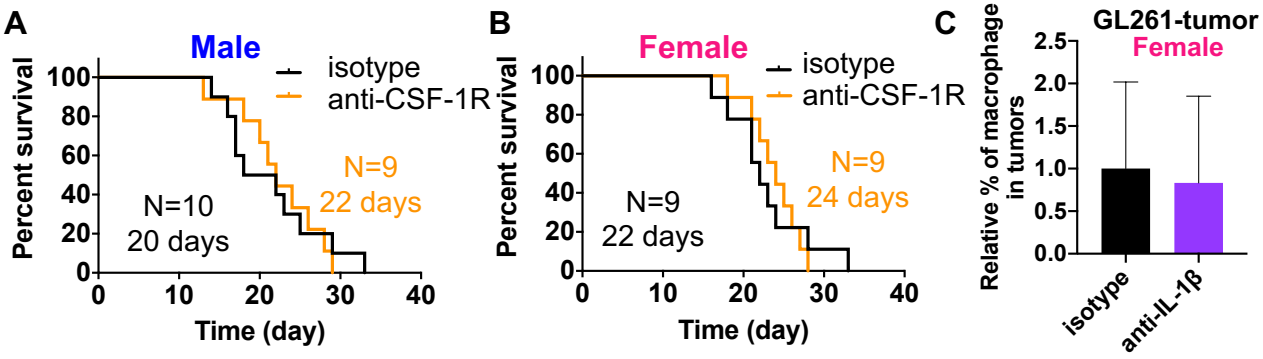

Supplementary Figure 9. Macrophages have limited contribution to the sexual dimorphism in GBM immune response. Kaplan-Meier curves depicting survival of **A,** male and **B,** female treated with anti-CSF-1R neutralizing antibody every other day starting 7 days post-GL261 implantation compared to isotype-treated mice. Data presented from two independent experiments with (**A**) n = 10 isotype-treated males and n = 9 anti-CSF-1R-treated males, (**B**) n = 9 isotype-treated females and n = 9 anti-CSF-1R-treated females. **C,** Relative frequency of tumor-infiltrating macrophages from n = 8 isotype- and n = 8 anti-IL-1β-treated GL261-bearing female mice. Data shown as mean ± s.d. from two independent experiments and normalized to isotype control.